JOURNAL OF CATALYSIS 134, 13–23 (1992)

Transient Response Study of CO Insertion into CH_x Surface Intermediates on a Vanadium-Promoted Rhodium Catalyst

TIJS KOERTS AND RUTGER A. VAN SANTEN

Schuit Institute of Catalysis, Department of Chemical Engineering, Eindhoven University of Technology, PO Box 513, 5600 MB Eindhoven, The Netherlands

Received March 4, 1991; revised July 22, 1991

The rate of CO insertion into surface CH_x species was investigated on silica-supported rhodium and rhodium–vanadium catalysts. Isotopically labelled ^{13}CO was used in a transient kinetic experiment under steady-state conditions. A main conclusion is that vanadium promotion does not affect the rate of CO insertion. From temperature-programmed surface reaction measurements the surface concentration of CH_x species during steady-state reaction was determined. It is increased by vanadium coadsorption. Combining these data with the selectivity and activity in synthesis gas to oxygenate conversion, a model is derived from which reaction rates of elementary steps and surface concentrations are calculated. Ethanal formation appears to occur at two distinguishable sites. Vanadium promotion decreases the desorption rate of ethanal, enhances the hydrogenation rate to ethanol, and increases the surface concentration of oxygenated intermediates.

INTRODUCTION

The formation of oxygenated compounds such as ethanol and ethanal from synthesis gas is of significant fundamental interest (*1, 2*). Supported rhodium catalyses this reaction. Oxidic promoters like Mn_2O_3, FeO, V_2O_3, HfO_2, and TiO_2 have been shown to be necessary for high selectivity for ethanol formation (*3–7*). In the mechanism for the formation of ethanol and ethanal three main elementary reaction steps can generally be distinguished: CO dissociation, CO insertion into surface CH_x fragments, and hydrogenation of surface intermediates. The value of x in the CH_x species during CO insertion is equal to 3 or 2 (*8*) because only then can the metal–carbon interaction be considered small enough (*9*) to allow CH_x species mobility so that CO insertion is possible. CO insertion leads to a reaction intermediate which can produce ethanol and ethanal. This is indicated in the general reaction scheme of Fig. 1.

Orita *et al.* (*10*) have shown that the formation of ethanal occurs from an acetate species as reaction intermediate. Underwood and Bell (*11*) and Kiennemann *et al.* (*12*) showed that ethanal is the precursor for ethanol formation. Jackson *et al.* (*13*) suggested that different reaction intermediates are responsible for ethanol and ethanal formation, because ethanal formation is much faster than ethanol formation. This was deduced from experiments in which ^{13}CO was pulsed in a synthesis gas flow. Contrary to this finding, Ichikawa and Fukushima (*14*) showed, by a reaction of ^{13}CO and $^{13}CH_3OH$ with synthesis gas, that ethanal and ethanol can be generated from a common reaction intermediate. Fukushima *et al.* (*15*) indicated this reaction intermediate as an acyl species from FT–IR spectroscopy. In addition to such a reaction intermediate a second oxygenated reaction intermediate must be proposed in the reaction mechanism of Fig. 1, which can be an ethoxy species as shown by the same authors (*15*). This intermediate was also proposed by Agarwal *et al.* (*16*), who studied the hydrogenation of ethanal to ethanol. They argued that ethanal adsorbs on the catalytic active surface through the oxygen atom and is hydrogenated to an intermediate

0021-9517/92 $3.00

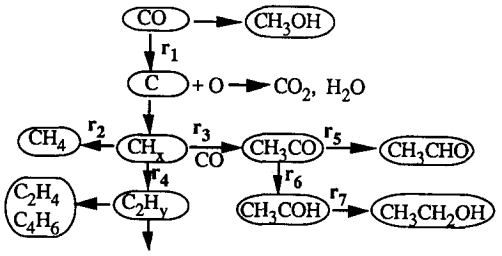

FIG. 1. Elementary reaction scheme for synthesis gas conversion into oxygenates (*10–16*).

which is bonded by its hydroxy carbon atom to the metal surface. Although it remains unclear whether the first oxygenated reaction intermediate (CH_3CO) is adsorbed as an acyl species or as acetate, and whether the second oxygenated intermediate (CH_3COH) is bonded through a carbon atom or an oxygen atom to the surface, the transient data show that at least two different reaction intermediates must be taken into account.

The influence of promoters on the rate of CO dissociation has been studied extensively (*17–19*). Both alkali and oxygen-containing species from transition metals can enhance the rate of CO dissociation. The enhanced CO dissociation rate, as demonstrated for vanadium promotion (*20, 21*), will increase the overall activity of a rhodium catalyst with respect to the synthesis gas conversion reaction. Much less is known about the effect of promoters on the CO insertion rate into adsorbed CH_x species. Fukuoka *et al.* (*22, 23*) recently suggested a mechanism for iron-promoted rhodium catalysts in which tilted adsorbed CO molecules resulted in an enhanced activity for CO insertion. From activity measurements, Chuang *et al.* concluded that CO insertion is favoured by small metal ensembles, which could be created by blocking silver atoms (*24*) or by coadsorbed sulfur (*25*). The results of CO insertion activity obtained from ethylene addition to synthesis gas resulting in propanol (*26–29*) must be interpreted cautiously. Ethylene addition will also change the surface concentration of reaction intermediates, which may affect selectivities. Orita *et al.* (*10*) showed that potassium oxide could supply reactive oxygen, which can be used to stabilise acetate species. This was also shown by Fukushima *et al.* (*30, 15*) with FT–IR measurements on vanadium-promoted rhodium in a similar way for acyl species. Also Boujana *et al.* (*31*) noted a stabilised acetyl species when a promoter is added to a paladium catalyst. A relation has been proposed between the stabilisation of oxygenated intermediates and an improved selectivity for ethanol formation. Despite all these suggestions, a direct study of the reactivity of adsorbed CH_x fragments with CO has not yet been performed. Here we report on a study of the CO insertion step under steady-state conditions using transient kinetic experiments.

Steady-state isotopic transient kinetic analysis (SSITKA), as introduced by Happel, is a powerful tool to analyse reaction rates of elementary steps and has been used by several groups (*32–37*). Without changing the steady-state conditions it is possible to determine surface concentrations of reaction intermediates and their residence times on the catalyst surface. Also the heterogeneity of the surface can be analysed, as is shown for the formation of ethanal.

The effect of vanadium promotion on a silica-supported rhodium catalyst was studied for the reaction of surface CH_x and CO to an adsorbed CH_3CO intermediate and its subsequent hydrogenation. The enhancement of CO dissociation by vanadium promotion (*38, 39*) complicates direct analysis of the transient data. To circumvent this we analysed the incorporation rate of ^{13}C from CO into the carbonyl group of ethanal and into the hydroxy-carbon group of ethanol during a stepwise change from ^{12}CO synthesis gas to labelled ^{13}CO.

$$H_2 + CH_x + {}^{13}CO \rightarrow CH_3{}^{13}\mathbf{C}HO + CH_3{}^{13}\mathbf{C}H_2OH. \quad (1)$$

The ^{13}C carbon atoms (boldface) in ethanal

and ethanol are from undissociated CO, and the rate of incorporation will be independent of the rate of CO dissociation. The incorporation of these ^{13}C atoms can be detected by analysing mass spectra.

The rate of appearance of ^{13}CO in products will not only depend on the rate of CO insertion, but also on the rate of hydrogenation of the adsorbed CH_3CO intermediates and on their subsequent rate of desorption. To analyse the interactions of ethanal and ethanol precursors with the catalyst, we carried out temperature-programmed desorption (TPD) experiments. The hydrogenation rate of surface intermediates was studied in a separate experiment in which ethanal was hydrogenated to ethanol.

The results are analysed using a model in which the influence of the vanadium promoter is described in terms of changes in reaction rates of the elementary steps and surface concentrations of reaction intermediates. In order to do so, the surface concentration of adsorbed CH_x intermediate must be known. The concentrations were estimated from separate temperature-programmed surface reaction (TPSR) experiments, using the observation that the reactivity of adsorbed CH_x intermediates in hydrogenation is much higher than that of adsorbed CO (*39, 40*).

EXPERIMENTAL

Catalyst

A 3 wt% rhodium catalyst was made by pore volume impregnation of preshaped Grace 332-type silica (surface area = 300 m^2/g, mesh size = 100) with an aqueous solution of $RhCl_3$. After reduction at 350°C for 16 h and passivating at room temperature, vanadium was added by post-impregnation of a solution of ammonium metavanadate. On the promoted catalyst the mol ratio of rhodium : vanadium was 3. The amount of CO that can be chemisorbed on the promoted catalyst system was rather insensitive for the reduction temperature. The vanadium promoter covered the rhodium particles as deduced from CO chemisorption and other techniques (*39*). From transmission electron microscopy photographs it was concluded that the rhodium particles have the same size on both catalysts.

Method

Prior to each experiment, the catalyst was reduced *in situ* at 350°C for at least 1 h. Catalytic reaction was carried out with 500 mg of the catalyst in a flow of 15 ml/min of synthesis gas (H_2/CO = 2) at 210°C. All experiments were performed after 1 h of steady-state synthesis gas reaction.

With TPSR the surface concentration of reactive surface carbon species during synthesis gas reaction was determined. After the synthesis gas reaction the reactor was quickly cooled to 100°C in a helium flow, while CH_x intermediates as well as CO remained adsorbed. At 100°C only the reactive CH_x intermediates produce methane in a reaction with hydrogen. On raising the temperature surface carbon monoxide and graphitic carbon are hydrogenated to methane. The amount of methane produced at 100°C divided by the total amount of methane produced in a TPSR experiment was used as an estimate for the concentration of adsorbed surface CH_x intermediates.

For the transient kinetic experiment a reactor system equipped with a mass spectrometer was used. All dead volumes were minimised. The dead volume of the reactor above the catalyst was filled with quartz. Just above the reactor a four-way valve could switch from normal synthesis gas to ^{13}C-labelled synthesis gas. After the catalyst bed a small tube led to a multiposition 16-way loop valve (type ST16 Chrompack). This valve contained 16 loops of 0.3 ml which could be placed in turn into the reaction gas flow. By switching this valve, 15 loops of reaction gas could be stored. It was kept at 110°C. To obtain well-defined response data without disturbing the steady state, it is important that the pressures are the same in the two flow sets before switching. The pressure drop of the catalyst bed (normally about 0.18 atm) was also created

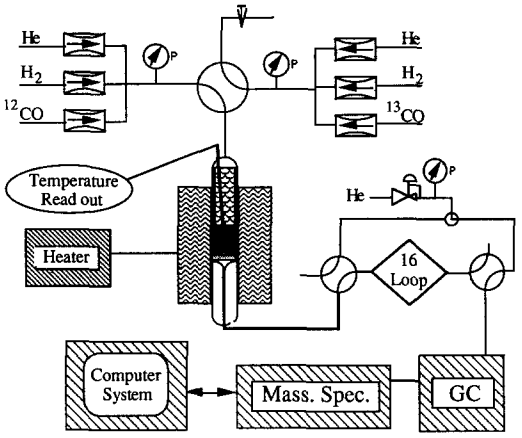

FIG. 2. Schematic presentation of the time-based GC–MS equipment as used for the isotopic transient experiment.

in the second flow by a needle valve. The system is schematically presented in Fig. 2.

The temperature in the catalyst bed was measured by a thermocouple in a quarts capillary. After 1 h of steady-state reaction, the synthesis gas was switched to labelled ^{13}CO (MSD isotopes, 99.3% ^{13}C). Reaction continued and 15 loops of reaction gas were subsequently stored. Afterwards the stored gases were pulsed into a gas chromatograph on a widebore plot q column 13 m long (ϕ = 0.53 mm). All components, except methane, hydrogen, and CO, were separated in a temperature-programmed GC run from 30 to 180°C. The widebore column was connected by a glass press-fit coupling with a capillary column of 3 m length which introduced the components into a high-resolution mass spectrometer (AMD MMH1, Harpstedt, Germany (*41*)). Every 1.5 s all masses between 10 and 50 atomic mass units were measured. The data were stored in a computer system and evaluated afterwards with a DP 1.05 program. From the fragment ions in the mass spectrum it was possible to calculate the fraction of labelled ^{13}C in the carbonyl group of ethanal from masses 29 and 30 and in the hydroxy-carbon group of ethanol from masses 31 and 32. Corrections were made for the natural fragmentation of the products, the oxygen and nitrogen background, and the natural abundance of ^{13}C of 1.1%. The transient experiment was duplicated.

The hydrogenation of ethanal to ethanol was tested in a microflow reactor (i.d. 10 mm). A flow of 58 ml/min of 2% ethanal and 8.5% hydrogen in helium was passed over 300 mg of the reduced catalysts at different temperatures. The products were analysed with a gas chromatograph (Chrompack, CP 9000), using a widebore plot q column of 25 m length (ϕ = 0.53 mm). The TPD experiments were performed in the same reactor system. The catalyst was saturated with ethanal or ethanol by adsorption in a helium flow of 56 ml/min at 110°C. After flushing for 30 min in helium the reactor was cooled to 40°C and the TPD was started in a helium flow of 20 ml/min. The temperature was raised at 5°C/min while every 2 min the desorbing products were analysed with the GC.

RESULTS

The activity and selectivity of the catalysts during the steady-state synthesis gas reaction are presented in Table 1. As previously noted (*20, 21, 38, 39*) the vanadium promoter shifts the selectivity from ethanal to ethanol. The overall activity is about four times increased.

The transient response curves of the incorporation of ^{13}C into ^{13}CO to produce $CH_3{}^{13}CHO$ and $CH_3{}^{13}CH_2OH$ for the rho-

TABLE 1

Activity and Product Distribution during Synthesis Gas Reaction at 210°C (H_2/CO = 2, 1 atm) of the Rhodium and the Rhodium–Vanadium Catalysts

Catalyst	Activity TON[a]	Selectivity (%)				
		Ethanal	Ethanol	Methane	C_2^+ H.C.	oxo's
Rh	0.27	7.18	18.9	42.0	25.0	6.9
RhV	1.00	2.28	22.8	36.3	29.8	8.8

[a] Activity expressed as mmol CO converted per surface metal atom per second.

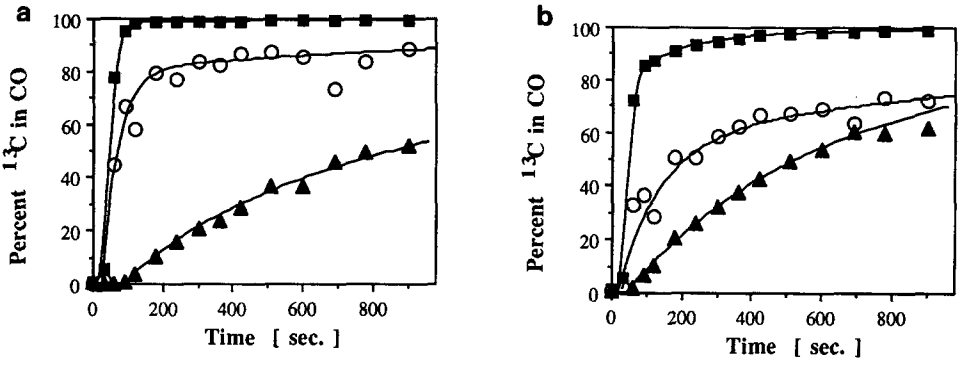

FIG. 3. Appearance of ^{13}C from ^{13}CO in carbon monoxide (squares), the carbonyl group of ethanal (circles) and in the hydroxy-carbon group of ethanol (triangles). (a) Rhodium. (b) Rhodium–vanadium.

dium and rhodium–vanadium catalyst are presented in Figs. 3a and 3b.

The disappearance with time of the fraction of ^{12}C in the above-mentioned carbon atoms of ethanal and ethanol for the Rh and RhV catalysts is shown on a logarithmic scale in Fig. 4. The presence of the vanadium promoter slows the rate of ^{13}C incorporation into ethanal while it is enhanced in ethanol.

Differences in the interaction of ethanal and ethanol with the silica support follow from the TPD curves of Fig. 5. Ethanal and ethanol TPD experiments from the Rh and RhV catalysts were also carried out, showing a rate of decomposition of ethanal and ethanol higher than that of the pure silica.

To compare the normalised rate of CO insertion on the Rh and RhV catalysts, the surface concentration of reactive surface carbon is required. This was analysed with a TPSR experiment (Fig. 6). The total amount of hydrogenatable surface species on the RhV catalyst is about half of that on the Rh catalyst, due to partial coverage of the rhodium particles by the promoter. The concentration of reactive carbon species is determined from the amount of methane produced at 100°C divided by total amount of methane formed (up to 400°C) and is

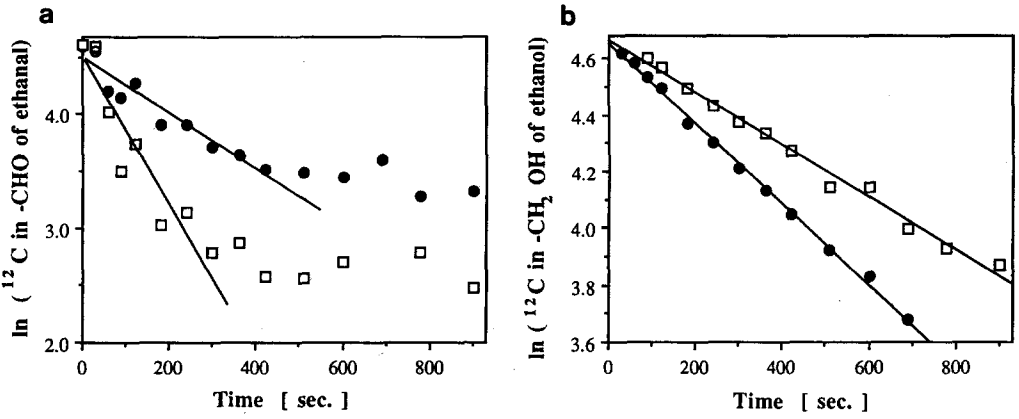

FIG. 4. The disappearance of ^{12}CO in C_2 oxygenates compared on the rhodium (squares) and rhodium–vanadium (circles) catalysts. (a) Ethanal. (b) Ethanol.

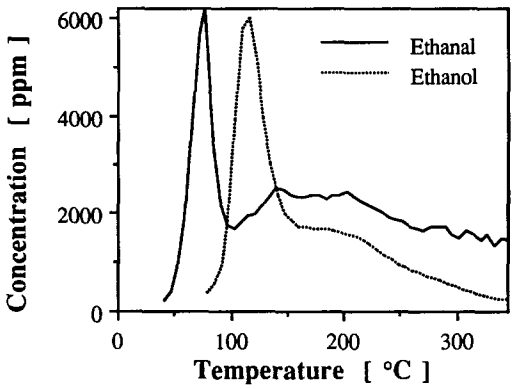

FIG. 5. Temperature-programmed desorption of ethanal and ethanol from silica (ethanol concentration is multiplied by 3).

0.34% for the Rh catalyst and 1.4% for the RhV. The low concentration of the reactive C_α carbonaceous intermediates corresponds well with the amount found by Efstathiou and Bennett (*40*).

Finally we analysed the influence of the vanadium promoter on the hydrogenation of ethanal to ethanol in a separate experiment. The activity and selectivity as well as the order in ethanal and hydrogen are presented in Table 2 and Fig. 7. It can be seen that both activity and selectivity to ethanol are greatly increased by the vanadium promoter. The activation energy for ethanal

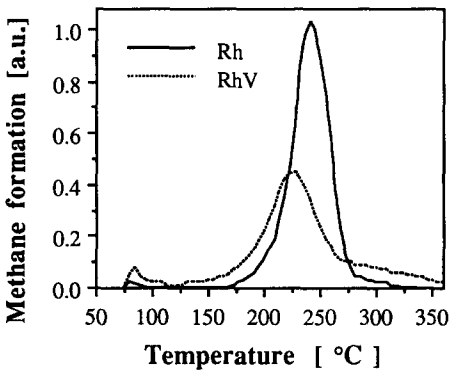

FIG. 6. Temperature-programmed hydrogenation of surface species formed during 1 h of synthesis gas reaction.

TABLE 2

Activity and Selectivity for Hydrogenation of Ethanal to Ethanol at 110°C

	Activity TON[a]	Ethanol selectivity (%)	Order in hydrogen	Order in ethanal	Deactivation (%/h)
Rh/SiO_2	0.114	65	1.70	−0.5	4
RhV/SiO_2	0.965	93.3	0.80	−0.4	1

[a] Mol converted ethanal per surface rhodium atom per second.

conversion is hardly changed: 44 kJ/mol for Rh and 43 kJ/mol for RhV.

DISCUSSION

The incorporation rates of ^{13}C correspond well with the results of Jackson *et al.* (*13*) on Rh/SiO_2. They pulse-labelled ^{13}CO and $C^{18}O$ into a synthesis gas flow and measured the incorporation into ethanal and ethanol. They noted that the incorporation into ethanal is very fast while the incorporation into ethanol was so slow that it could not be observed.

Analysis of the SSITKA data presented in Fig. 3 permits one to quantify the heterogeneity of the surface. A semilogarithmic plot of the normalised isotopic transient data is expected to be linear. However, for the formation of ethanal, a clear deviation exists from straight line behaviour (Fig. 4) at higher response times. The total turnover frequency (TOF) of a first-order surface reaction taking place on a nonhomogeneous surface can be modelled as a sum of exponentials. The distribution of the rate constant k can be estimated by fitting the transient curve with

$$\mathrm{TOF} = \theta_0 \sum_i (x_i k_i e^{-k_i t}). \qquad (2)$$

θ_0 is the total surface coverage, and x_i is the fraction with reactivity k_i. De Pontes *et al.* (*36*) derived a general deconvolution to extract the function $x(k)$. For less well-defined data one can also model the transient data using Eq. (2). Fixed k values were chosen and the amplitudes were fitted. The k-value

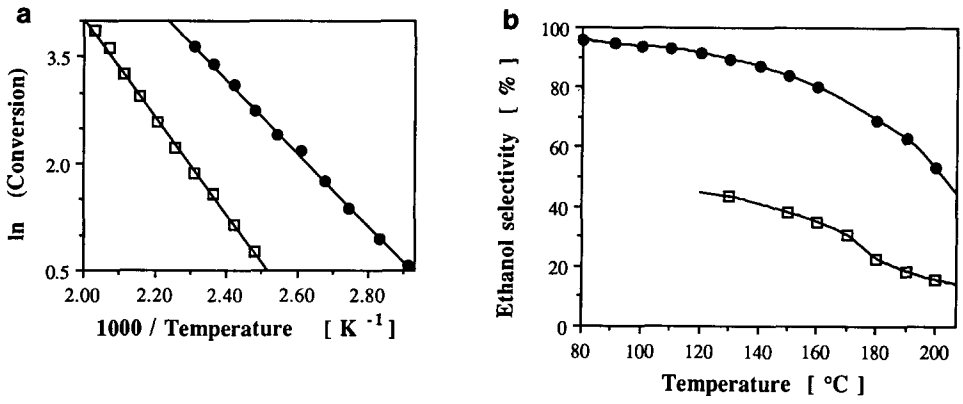

FIG. 7. Hydrogenation of ethanal to ethanol on the rhodium (squares) and rhodium–vanadium (circles) catalysts. (a) Arrhenius plot. (b) Selectivity.

distributions derived from the Rh and RhV catalyst are shown in Fig. 8. The incorporation rate calculated from this figure is shown as the fit in Figs. 3a and 3b. One concludes that ethanal formation occurs at least at two different sites. Vanadium promotion decreases the reactivity of the active sites and increases the fraction of stabilised ethanal intermediates which desorb only slowly as ethanal.

To obtain quantified information from the plots in Figs. 3a and 3b, in terms of elementary reaction rates, we used the kinetic scheme as shwon in Fig. 1. Also the surface concentrations of the reaction intermediate

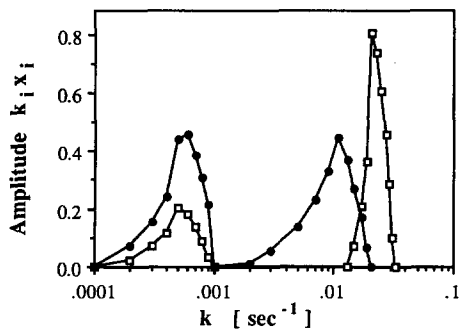

FIG. 8. Distribution of the reactivity constant k for ethanal formation on the rhodium (squares) and rhodium–vanadium (circles) catalysts as deduced from the isotopic transient kinetic data.

CH_3CO and CH_3COH can be calculated. The hydrogen dependence of each elementary step is not explicitly considered. Our analysis implicitly assumes that the hydrogen partial coverage is constant. The two important oxygenated reaction intermediates from Fig. 1 are presented as $I_1 \equiv \theta_{CH_3CO}$ and $I_2 \equiv \theta_{CH_3COH}$. To extract the r values, the necessary equations must first be deduced. For incorporation of ^{13}C into the aldehyde group of ethanal according to the mechanism from Fig. 1, one can write the rate equations

$$\frac{d\mathrm{CH_3{}^{13}CHO}}{dt} = r_5\, {}^{13}I_1 \qquad (3)$$

$$\frac{d^{13}I_1}{dt} = r_3\theta_{CH_3}^{\alpha}\theta_{^{13}CO}^{\beta} - (r_5 + r_6)\, {}^{13}I_1. \qquad (4)$$

The reaction orders α and β of the surface intermediates are assumed to be one. The integration of (4) results in

$$ {}^{13}I_1(t) = \frac{r_3\theta_{CH_3}}{r_5 + r_6}[1 - e^{-(r_5+r_6)t}] - \frac{r_3\theta_{CH_3}}{\gamma - (r_5 + r_6)}[e^{-(r_5+r_6)t} - e^{-\gamma t}]. \qquad (5)$$

In this equation γ is introduced as a correction for the nonideal switch from ^{12}CO to ^{13}CO, which can be deduced from the experimental data in Figs. 3a and 3b. For large γ

(stepwise change from ^{12}CO to ^{13}CO) the second part of this equation becomes zero. The measure γ values were 0.05 s^{-1} for the Rh and 0.03 s^{-1} for the RhV experiment while the dead time for response was 27 s. The scrambling between adsorbed ^{12}CO and ^{13}CO gas is rapid, as concluded by Yates *et al.* (*42*).

The rate of ^{13}CO incorporation into the aldehyde function of ethanal follows from Eqs. (3) and (5).

$$CH_3{}^{13}CHO(t) = \frac{r_5 r_3 \theta_{CH_3}}{r_5 + r_6}[1 - e^{-(r_5+r_6)t}] - \frac{r_5 r_3 \theta_{CH_3}}{\gamma - (r_5 + r_6)}[e^{-(r_5+r_6)t} - e^{-\gamma t}]. \quad (6)$$

The incorporation of ^{13}C into the hydroxy-carbon group of ethanol can be deduced in the same way according to the mechanism of Fig. 1.

$$\frac{d^{13}CH_3CH_2OH}{dt} = r_7\, {}^{13}I_2(t). \quad (7)$$

$$\frac{d^{13}I_2}{dt} = r_3\, {}^{13}I_1(t) - r_7\, {}^{13}I_2(t). \quad (8)$$

The solution for $I_2(t)$ is presented in (9) assuming $\gamma \gg k_5 + k_6$, which is valid because the incorporation of ^{13}C in CO is much faster than that in ethanol as shown in Fig. 3.

$$^{13}I_2(t) = \frac{r_6 r_3 \theta_{CH_3}}{r_7(r_5 + r_6)}\left[1 - \frac{r_7}{r_5 + r_6 - r_7}e^{-(r_5+r_6)t} - \left(1 - \frac{r_7}{r_5 + r_6 - r_7}\right)e^{-r_7 t}\right]. \quad (9)$$

Equations (7) and (9) produce the desired equation

$$CH_3{}^{13}CH_2OH(t) = \frac{r_6 r_{3\,CH_3}}{r_5 + r_6}[1 - Ke^{-(r_5+r_6)t} - (1 - K)e^{-r_7 t}] \quad (10)$$

for the rate of appearance of ^{13}C into ethanol, in which $K = r_7/(r_5 + r_6 - r_7)$.

For the analysis of the rate constants according to Eqs. (6) and (10) only the reactive sites for ethanal formation are taken into account. The experimental data of ^{13}C incorporation into ethanal is fitted with formula (10). The fitted curves are shown in Fig. 3b. The resulting k values: $k_5 + k_6$ and k_7, are presented in Table 3. At high response time the calculated ethanal curve becomes higher than the measured one (Fig. 3b). This can be corrected if the slow sites for ethanal formation are also taken into account in Eq. (10). However, at residence times lower than 750 s, the transient data can be explained within experimental error. This supports the chosen mechanism. The deduced rate parameters from these fits are presented in Table 3.

TABLE 3

Changes in Reaction Rates and Surface Concentrations of C_2O Intermediates by Vanadium Promotion at 210°C

	$r_3{}^a$	$r_5{}^a$	$r_6{}^a$	$r_7{}^a$	θC_2O^b	θC_2OH^b
Rh	22	5.7	15	0.83	0.003	0.06
RhV	20	0.95	10	1.2	0.024	0.18
RhV/Rh	0.9	0.17	0.7	1.5	7.2	3.0

[a] r as TOF: mmol converted product per second per mol reaction intermediate.
[b] Surface concentration θ in rhodium fraction covered.

The reaction rate constants r_3, r_5, r_6, and r_7, as well as the surface concentration of the reaction intermediates I_1 and I_2, can be calculated for both the rhodium and the vanadium-promoted catalyst from a more complete analysis. Therefore six independent equations must be solved. The necessary information is obtained from the selectivities and turnover numbers (TON) from Table 1 and the surface concentration of CH_x intermediates, which has been estimated with TPSR. The first two equations are (6) and (10). The other equations can be solved using the steady-state assumptions

$$\frac{r_5}{r_6} = \frac{\text{ethanal selectivity}}{\text{ethanol selectivity}} \quad (11)$$

$$r_3\theta_{CO}\theta_{CH_x} = I_1(r_5 + r_6) \quad (12)$$

$$I_1 r_5 = \text{TON selectivity ethanal} \quad (13)$$

$$I_2 r_7 = \text{TON selectivity ethanol.} \quad (14)$$

The resulting rate parameters for the rhodium and vanadium-promoted rhodium catalysts are presented in Table 3.

Residence times of surface intermediates may be affected due to chemical interaction of C_2O or C_2OH intermediates with the silica support. The following equilibrium must be considered especially

$$\text{Si–OH} + \text{HOCH}_2\text{CH}_3 \Leftrightarrow \text{SiOC}_2\text{H}_5 + \text{H}_2\text{O}. \quad (15)$$

To ensure that the long residence time of ethanol intermediates is not due to a great buffer of C_2OH intermediates adsorbed on the silica carrier, TPD experiments were performed. In Fig. 5 it is shown that most of the chemisorbed ethanal and ethanol will desorb below 210°C, the reaction temperature during steady-state experiments. Moreover, during synthesis gas reaction, the concentration of water is about three times greater than that of ethanol, which shifts the equilibrium of Eq. (14) to the left. Thus it is unlikely that long residence times of ethanol are due to an interaction with the silica support. However, for ethanal desorption it cannot be excluded that the unreactive sites (Fig. 8) for ethanal formation are responsible for an interaction with the silica support because some ethanal formation also occurs at temperatures above 210°C.

The TOF for CO insertion from Table 3 on the Rh and RhV catalyst differ by only 10%. CO insertion is fast compared with the hydrogenation steps and is therefore not rate limiting. This reaction step can be considered to be in local equilibrium because the reverse reaction, the decomposition of a C_2O intermediate to CO and CH_x, is also fast on rhodium catalysts. This follows from TPD experiments by Davis and Barteau (*43*). Coadsorption of vanadium makes the CH_x fragments a little less reactive for CO insertion. The enhancement for CO insertion through oxidic promoters, as measured in homogeneous catalysis (*44, 45*), is not valid for the discussed heterogeneous RhV system.

An increase in the selectivity towards more C_2 oxygenates through oxidic promotion is not due to an enhanced CO insertion activity, but can be due to a stabilisation of oxygenate intermediates. This shifts the CO insertion equilibrium to adsorbed oxygenates. Further, oxoselectivity can be increased through a decrease in the reactivity of the CH_x intermediates towards methane, as discussed before (*46*). The stabilisation of the C_2O intermediates appears from the increased surface concentration of these surface species through vanadium promotion. The stabilisation of acetate species during the synthesis gas reaction has been observed with infrared spectroscopy (*47, 48*). However, Orita *et al.* (*47*) mentioned that not all the observed acetate species are reaction intermediates because they do not disappear upon hydrogenation. Also Bastein (*48*) could not estimate which part of the reaction intermediates is able to react towards ethanol or ethanal. The same is valid for the FT–IR work of Fukushima *et al.* for acyl species (*15*). In our experiment we only account for those CH_3CO species that are true reaction intermediates because they are calculated from the TOF. For the mechanism of acetate stabilisation, Orita *et al.* (*10*) showed that one oxygen atom of the support is needed. Similarly, it can be proposed that vanadium can act as an oxygen donor, which can increase the number of stabilised oxygenated intermediates. Also the ionic V–O bonds can influence the metal particles, resulting in a more polar rhodium surface. This can result in more strongly adsorbed oxygen-containing intermediates.

Orita *et al.* (*10*) suggested that acetate species are located at the support near the rhodium metal particles. The high surface coverage of oxygenated reaction intermediates as calculated in Table 3 also suggests that at least part of these species are not located on the rhodium particles. Especially in the presence of vanadium, the high sur-

face concentration of oxygenated intermediates suggests that CH_3CO species are possibly located on the vanadium or on the silica support near the rhodium particles. From the heterogeneity in the residence time of ethanal intermediates one can speculate that the reactive ethanal species are created on the rhodium particles while the less reactive ones are slowly desorbing from the silica support. This was also suggested by Arakawa *et al.* (*50*) who noted two different acetate species with *in situ* IR spectroscopy during synthesis gas conversion at 50 atm at 260°C.

Table 3 shows that during the synthesis gas reaction the hydrogenation rate to ethanol is increased by vanadium promotion, as was also found for cerium oxide promotion by Kiennemann *et al.* (*12*), for molybdenum promotion by Jackson *et al.* (*51*), and for tungsten promotion by Bhore *et al.* (*52*). This is more obvious from the separate hydrogenation experiment of ethanal to ethanol (Figs. 7a and 7b). From these figures it appears that the hydrogenation activity is increased by a factor of 9 without changing the activation energy. The enhanced activity seems to be due to a greater number of active hydrogenation sites. The reaction order during hydrogenation of ethanal to ethanol is a little negative in ethanal and positive in hydrogen, suggesting a stronger adsorption of ethanal than hydrogen. Remarkable is the decrease in the reaction order in hydrogen from 1.7 to 0.8 through vanadium. This can be due to stronger adsorbed hydrogen. This effect is in agreement with effects induced by spillover hydrogen as reported in Refs. (*51, 52*). Also the selectivity for methane formation is decreased during ethanal hydrogenation. This effect is due to the smaller size of rhodium metal ensembles on the RhV system because the vanadium promoter is on top of the rhodium particles. This decreases the rate of C–C bond scission, which is known to be a structure-sensitive reaction. This is in agreement with the reduced activity for hydrogenolysis of ethylene to methane through vanadium on this catalyst as reported in Refs. (*38, 49*).

CONCLUSION

The influence of vanadium promotion on the kinetics of several elementary reaction steps was studied by a steady-state isotopic transient kinetic analysis experiment. On the basis of the transient data, a kinetic model based on elementary reaction steps is proposed. It appears that the residence time of oxygenated intermediates on the catalyst surface reacting to ethanal is much smaller than intermediates reacting to ethanol. Vanadium promotion reduces the residence time of ethanol intermediates, while it enhances the residence time for ethanal intermediates. The turnover frequencies for CO insertion are high compared with hydrogenation rates and CO insertion is not a rate-limiting step. Vanadium promotion does not promote CO insertion.

Ethanal formation occurs at least at two different sites. Vanadium promotion stabilises oxygenated reaction intermediates on the catalyst surface, which results in a decrease of the rate of ethanal desorption. The hydrogenation activity of oxygenated intermediates to ethanol is enhanced by vanadium, which can be explained by more strongly adsorbed hydrogen.

ACKNOWLEDGMENTS

We gratefully thank Professor Dr. G. B. M. M. Marin for the opportunity to use his reactor system with the 16-way loop valve and Dr. P. A. Leclercq and H. Snijders for the use of and assistance with the high-resolution mass spectrometer, which made the transient response study possible. Further we acknowledge Johnson and Matthey for the free use of their high-purity rhodium chemicals. Finally we thank the Dutch organisation of fundamental chemical research, SON, for its financial support.

REFERENCES

1. Katzer, J. R., Sleight, A. W., Gajardo, P., Michel, J. B., Gleason, E. F., and McMillan, S., *Faraday Discuss. Chem. Soc.* **72**(8), 121 (1981).
2. Gilhooley, K., Jackson, S. D., and Rigby, S., *Appl. Catal.* **21,** 349 (1986).
3. Nakajo, T., Sano, K., Matsuhira, S., and Arakawa, H., *Chem. Lett.* 1557 (1986).

4. Ichikawa, M., Shikakura, K., and Kawai, M., *in* "Heterogeneous Catalysis Related to Energy Problems," Proc. Symp. in Dalian, China, A.08-I (1982).
5. van den Berg, F. G. A., Glexer, J. H. E., and Sachtler, W. M. H., *J. Catal.* **93,** 340 (1985).
6. Bond, G. C., and Richards, D. G., *Appl. Catal.* **28,** 303 (1986).
7. Bhasin, M. M., Bartley, W. J., Ellgen, P. C., and Wilson, T. P., *J. Catal.* **54,** 128 (1987).
8. Hackenbruch, J., Keim, W., Röper, M., and Strutz, H., *J. Mol. Catal.* **26,** 129 (1984).
9. Koerts, T., and van Santen, R. A., *Catal. Today,* in press.
10. Orita, H., Naito, S., and Tamaru, K., *J. Catal.* **90,** 183 (1984).
11. Underwood, R. P., and Bell, A. T., *Appl. Catal.* **21,** 157 (1986).
12. Kiennemann, A., Breault, R., and Hindermann, J-P., *J. Chem. Soc. Faraday Trans. 1* **83,** 2119 (1987).
13. Jackson, S. D., Brandreth, J. B., and Winstanley, D., *J. Catal.* **106,** 464 (1987).
14. Ichikawa, M., and Fukushima, T., *J. Chem. Soc. Chem. Commun.,* 321 (1985).
15. Fukushima, T., Arakawa, H., and Ichikawa, M., *J. Phys. Chem.* **89,** 4440 (1985).
16. Agarwal, A. K., Wainwright, M. S., and Trimm, D. L., *J. Mol. Catal.* **45,** 247 (1988).
17. Sachtler, W. M. H., Shriver, D. F., Hollenberg, W. B., and Lang, A. F., *J. Catal.* **92,** 429 (1985).
18. Solymosi, F., Tombácz, I., and Kocsis, M., *J. Catal.* **75,** 78 (1982).
19. Goodman, D. W., *Appl. Surf. Sci.* **19,** 1 (1984).
20. Kip, B. J., Smeets, P. A. T., van Wolput, J. H. M. C., Zandbergen, H., van Grondelle, J., and Prins, R., *Appl. Catal.* **33,** 157 (1987).
21. Bastein, A. G. T. M., Luo, H. Y., Mulder, A. A. J. P., and Ponec, V., *Appl. Catal.* **38,** 241 (1988).
22. Fukuoka, A., Kimura, T., Kosugi, N., Kuroda, H., Minai, Y., Sakai, Y., Tominaga, T., and Ichikawa, M., *J. Catal.* **126,** 434 (1990).
23. Fukuoka, A., Kimura, T., Rao, L-F., and Ichikawa, M., *Catal. Today* **6,** 55 (1989).
24. Chuang, S. C., Pien, S-I., and Narayanan, R., *Appl. Catal.* **57,** 241 (1990).
25. Chuang, S. C., Pien, S-I., and Sze, C., *J. Catal.* **126,** 187 (1990).
26. Chuang, S. C., Tian, Y. H., Goodwin, J. G., Jr., and Wender, I., *J. Catal.* **96,** 396 (1985).
27. Sachtler, W. M. H., and Ichikawa, M., *J. Phys. Chem.,* **90**(20), 4742 (1986).
28. Chuang, S. C., Goodwin, J. G., Jr., and Wender, I., *J. Catal.* **92,** 416 (1985).
29. Pijolat, M., and Perrichon, V., *Appl. Catal.* **13,** 321 (1985).
30. Fukushima, T., Arakawa, M., and Ichikawa, M., *J. Chem. Soc. Chem. Commun.,* 729 (1985).
31. Boujana, S., Demri, D., Cressely, J., Kiennemann, A., and Hindermann, J. P., *Catal. Lett.* **7,** 359 (1990).
32. Zhang, X., and Biloen, P., *J. Catal.* **98,** 468 (1986).
33. Nwalor, J. U., Goodwin, J. G., and Biloen, P., *J. Catal.* **117,** 121 (1989).
34. Iyagba, E. T., Hoost, T. E., Nwalor, J. U., and Goodwin, J. G., *J. Catal.* **123,** 1 (1990).
35. Hoost, T. E., and Goodwin, J. G., submitted for publication.
36. de Pontes, M., Yokomizo, G. H., and Bell, A. T., *J. Catal.* **104,** 147 (1987).
37. Siddall, J. H., Miller, M. L., and Delgass, W. N., *Chem. Eng. Commun.* **83,** 261 (1989).
38. Koerts, T., Welters, W. J. J., and van Santen, R. A., *J. Catal.* **133** (1992).
39. Koerts, T., Welters, W. J. J., van Santen, R. A., Nonnemann, L. E. Y., and Ponec, V., *in* "Proceedings, Conference on C1 Chemistry, Oslo, 1990."
40. Efstathiou, A. M., and Bennett, C. O., *J. Catal.* **120,** 137 (1989).
41. Leclerque, P. A., Snijders, H. M. J., Cramers, C. A., Maurer, K. H., and Rapp, U., *J. High Res. Chromatogr.* **12,** 651 (1989).
42. Yates, J. T., Duncan, T. M., Worley, S. D., and Vaughan, R. W., *J. Chem. Phys.* **70**(3), 1219 (1979).
43. Davis, J. L., and Barteau, M. A., *Surf. Sci.* **187**(2) 387, (1987).
44. Collman, J. P., Finke, R. G., Cawse, J. N., and Brauman, J. I., *J. Am. Chem. Soc.* **100,** 4766 (1978).
45. Richmond, T. G., Basolo, F., and Shriver, D. F., *Inorg. Chem.* **21,** 1272 (1982).
46. Koerts, T., and van Santen, R. A., *Catal. Lett.* **6,** 49 (1990).
47. Orita, H., Naito, S., and Tamaru, K., *J. Catal.* **112**(1), 167 (1988).
48. Bastein, A. G. T. M., Ph.D. thesis, Leiden University, 1988.
49. den Hartog, A. G., Deug, M., Jongerius, F., and Ponec, V., *J. Mol. Catal.,* in press.
50. Arakawa, H., Fukushima, T., Ichikawa, M., Takeuchi, K., Matsuzaki, T., and Sugi, Y., *Chem. Lett.,* 23 (1985).
51. Jackson, S. D., Brandreth, B. J., and Winstanley, D., *Appl. Catal.* **27,** 325 (1986).
52. Bhore, N. A., Sudhakar, C., Bischoff, K. B., Manogue, W. H., and Mills, G. A., *in* "9th International Congress on Catalysis, Calgary, 1988" (M. J. Phillips and M. Ternan, Eds.), Vol. 2, p. 594. Chem. Institute of Canada, Ottawa, 1988.